Guided-Mode Resonance and Plasmonic Array Structures for Enhanced Sensing

Introduction

Moxtek has achieved low cost, wafer-scale manufacturing of plasmonic, photonic crystal, and hybrid structures and is ready to support your production needs, from developmental projects through commercialization. Potential applications for these structures include label-free biosensing, surface enhanced Raman spectroscopy (SERS), and microarray-based surface enhanced fluorescence sensing (SEFS). This white paper presents label-free and microarray-based SEFS results for 1-D photonic crystal (PC) sensing utilizing the guided mode resonance (GMR) effect, as well as SERS sensing with 2-D metallic nano-dome arrays utilizing localized plasmonic hotspots.[1]

Experimental results for 1-D photonic crystal guided-mode resonance sensors

The metrology and modeling results depicted in Fig. 1a-1d are for a type of grating-coupled, leaky 1-D photonic crystal (PC) TiO_2 slab waveguide, also called guided mode resonance (GMR) filters,[2-3] which give a narrowband reflectance peak that is sensitive to the local refractive index above the grating. Four 1-D PC GMR sensor designs were fabricated with pitch varying from 360 - 410 nm, which allowed for spectral tuning of the resonance for SEFS and label-free sensing applications. Wafer-scale optical metrology tools were used to map out the reflectance uniformity of the GMR sensors using peak wavelength and peak height distributions (Figure 1c) before dicing, though existing tools were found to underestimate the quality of the structures and could not accurately resolve the narrower GMR linewidths (<10 nm FWHM). Chip-level measurement on the samples after dicing showed reasonable agreement with modeling and in some cases resonance quality factors (Q) >200 were observed (Fig. 1b), which can be controlled via grating duty cycle (DC), etch depth, and and TiO_2 slab waveguide thickness.

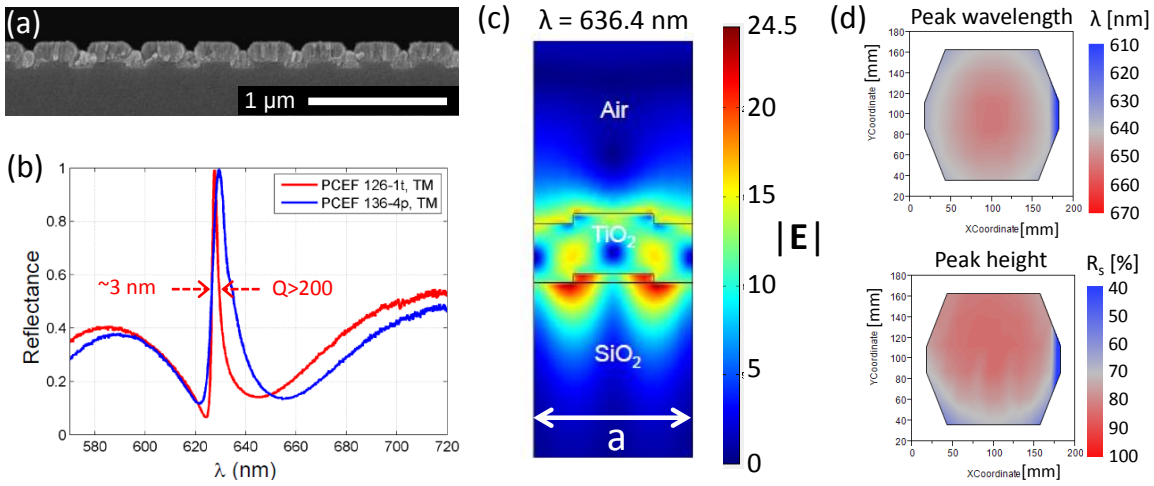

Figure 1. 1-D photonic crystal GMR characterization and modeling results: (a) SEM cross-section, (b) chip-level reflectance spectra, (c) optical model revealing near-field enhancement and field confinement near the grating layer, and (d) GMR sensor wafer-level reflectance maps showing uniformity of resonance position and peak height for a 200 mm diameter wafer.

The GMR structures were initially designed for use in an air environment and showed a large shift (~2.5 nm) in resonance position after binding a self-assembled monolayer (SAM) of n-octadecylphosphonate to the TiO2 waveguiding surface as a way to probe surface-sensing capability (Figure 2a). GMR filters also showed reasonable shift (~0.3 nm) during *in-situ* label-free sensing underwater in a flow cell configuration (Figure 2b), although some physical (non-covalent) SAM binding may also be taking place on the sample surface. The portion of the resonance shift attributed to covalent SAM formation within the liquid cell was estimated to be ~0.24nm. Spectral sensitivity on the order of 0.03 nm has been demonstrated using a similar GMR filter design on a smartphone-based spectrometer.[4] Hence sub-monolayer detection limits for moderately sized molecules are possible in these GMR sensor systems for label-free detection of surface binding events. These SAM binding studies demonstrate the potential of these GMR filter designs for use as compact label-free sensors, which could be based on either spectral shift in resonance position (as demonstrated), or changes in intensity. Moxtek is now developing PC-GMR designs optimized for in-situ biosensing in aqueous environments. By monitoring the spectral transmittance or reflectance in a properly designed system, these 1-D photonic crystal GMR devices are sensitive enough for applications such as enzyme-linked immunosorbent assays (ELISA) and both DNA and protein microarrays.[4-9]

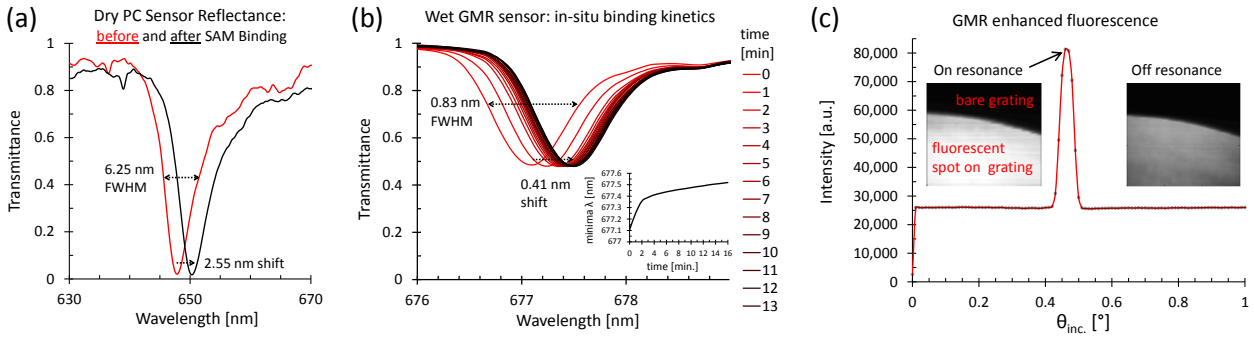

Figure 2. Proof-of-concept for 1-D photonic crystal GMR sensing applications. (a)-(b) Label-free SAM binding studies using transmittance of GMR 1-D photonic crystal structures on fused silica substrates. (a) Dry measurements in air before and after SAM binding procedure. (b) Label-free binding kinetics (inset indicates position of minima vs. time). (c) GMR-enhanced fluorescence intensity vs. excitation angle after spotting. The insets are fluorescence images when the angle is tuned on-resonance and off-resonance, and demonstrate GMR-enhanced fluorescence.

Greater than three-fold fluorescence intensity enhancement was also demonstrated (Fig. 2c) for a Cy-5 dye layer physisorbed to the surface of a filter when the excitation angle was tuned to match the GMR condition, though self-quenching may have limited the overall fluorescence output. The insets depict line-scan fluorescence images taken at the edge of the dye layer at angles of 0.46° (on resonance) and 2.0° (off resonance). The bright regions represent the dye layer while the dark regions have no dye whatsoever. Larger enhancement factors should be possible with improved laser beam alignment and collimation, and with narrower laser and GMR filter linewidths. In addition, by tuning the 1-D photonic crystal GMR design to enhance both laser excitation and fluorescence emission (utilizing TM *and* TE resonances), 60x -328x improvement in fluorescence detection sensitivity and 41-42x increase in signal-to-noise ratio have been demonstrated when compared to a reference slide.[6, 10]

GMR micro-arrays were then prepared using 1-D PC structures on Silicon substrates, where the resonance position was located near the excitation maxima of Cy-5 dye. IgG, IgM, IgA, and Streptavidin assays were performed by functionalizing the surface with an epoxy-silane and then covalently grafting the corresponding antigen via spotting at various concentrations followed by standard incubation and washing protocols. The fluorescently labeled antibodies were then introduced at various concentrations using a 16-well array to give a large array of fluorescence spots that were measured using standard fluorescence scanners. The Moxtek GMR substrates showed average enhancements of ~6.7 - 8.7 in the fluorescence signal minus local background when compared to a bare glass reference slide that underwent the same surface preparation and assay protocols. Similarly, for a bare silicon substrate that underwent the same surface preparation and assay protocols, the Moxtek GMR slides showed ~16.2 - 27.6 average enhancement. It should be noted that the commercial scanners utilized were not optimized for readout of these photonic crystal structures, which optimally would utilize a well-controlled illumination angle for the exciting source, as demonstrated in Figure 2(c). Current efforts are focused on building such an optimized line-scanning microscope for fluorescence assay readout of these GMR micro-array substrates.

Experimental results for 2-D SPR nano-dome array SERS sensors

The 2-D SPR nano-dome array structures, depicted in Fig. 3(a)-(b) below, were designed for SERS applications and utilize a localized surface plasmon hotspot between adjacent domes to generate large field enhancement. They were fabricated using 400 nm pitch SiO_2 posts that were conformally grown with additional SiO_2 before coating with gold. Performance is most sensitive to the nano-gap spacing between adjacent domes and the post height. The reflectance spectra for several experimental designs are given in Fig. 3(c). SERS measurements of Rhodamine 6G dye dried onto sample surfaces are given in Fig. 3(d), which compares background-corrected SERS spectra for a sample coated with rougher gold to that of one coated with smoother gold. The best SERS enhancement was observed for samples with the smoother gold coatings and ~15 nm nano-gaps. Similar SPR nano-dome array designs have been used to demonstrate point-of-care monitoring of intravenous drugs and metabolites, where one could potentially monitor and stop an infusion before a lethal dose of chemical reaches the patient, and where clinically relevant detection limits of 20-730 ng/ml were demonstrated.[11-13]

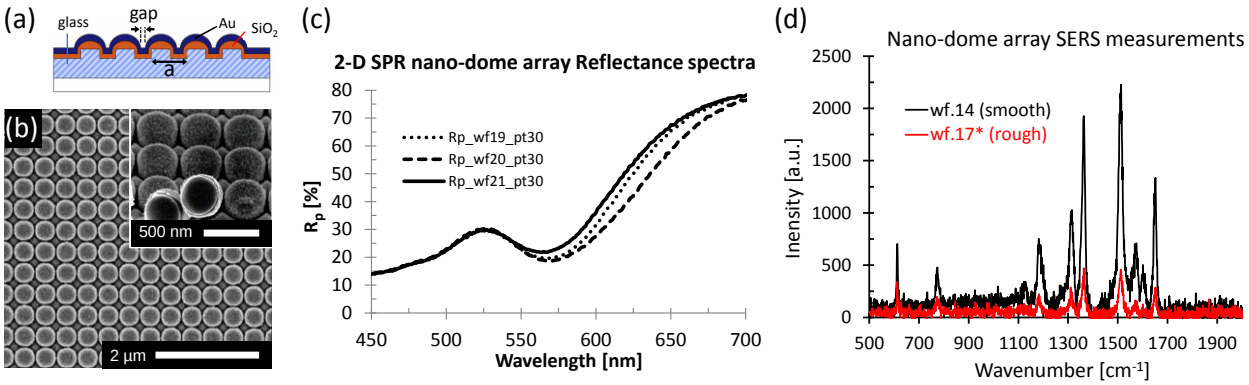

Figure 3. 2-D SPR nano-dome arrays for SERS applications. (a) Schematic cross section. (b) Plan view SEM with perspective view inset of broken sample. (c) Reflectance spectra. (d) SERS response for nano-domes with smooth and rough gold coatings.

The SERS response of Rhodamine 6G (R6G) was also measured on a glass reference slide, but no peaks were present, even after increasing both the laser power by a factor of 10 and the concentration by a factor of 1000. To get a measurable response, the sample was re-positioned away from the center of the dried R6G spot such that the laser was instead focused near the edge of the spot, where a coffee-ring-like drying effect produced even higher dye concentrations. From this region, weak Raman peaks were visible in the reference sample. The experimental (spatially averaged) SERS enhancement factor was then calculated as being at least 1.35 x 10^5, based on the ratio of measured Raman intensities at the 1363 cm^{-1} peak (16,230/1206), and corrected by the ratios of laser power and dye concentration for the two samples. This is an underestimate of the true enhancement factor, since the dye was further concentrated by a coffee-ring drying effect in the reference sample. Similar nano-dome array designs have shown 3.16 x 10^6 spatially averaged enhancement factor,[14] with local enhancement factors as large as 1.37 x 10^8. The larger, local enhancement factors are actually normalized by the ratio of the number of molecules within a hot-spot region to the number of molecules within an un-modified laser focal volume. This calculation assumes that most of the SERS signal is coming from a single hot spot between nano-dome arrays and describes only the enhancement that occurs within that region of highest electric field. It doesn't account for the experimental fact that only a portion of the available surface area of the substrate is supporting these hot spots. Hence the spatially averaged enhancement factor, in our case > 1.35 x 10^5, is the experimentally relevant parameter. This result for Au-coated nano-domes is within a factor of 23.4 of previous SERS results on silver-coated nano-dome arrays.[14] Current work is focused on evaluating the gold-coated nano-dome array performance using near-IR excitation, where Gold has improved optical properties.

Conclusions

A label-free biosensor designed for use as a microarray substrate showed ~2.5 nm shift in resonance position after monolayer binding. Wafer-scale uniformity maps were prepared and GMR quality factors exceeded 200 in some cases. Another PC-GMR design was developed for microarray-based SEFS and results from a non-optimized commercial scanner and non-optimized assay protocols produced ~7-28x signal enhancement when compared to reference slides. Furthermore, proper excitation source coupling was shown to produce better than three-fold enhancement of the fluorescence signal, which should lead to improved assay sensitivity with further substrate and scanner optimization. 2-D nano-dome arrays were also fabricated and showed sensitivity to the gap between adjacent nano-domes and to the roughness of the gold coatings. The experimental (spatially averaged) SERS enhancement factor was calculated as being greater than 1.35 x 10^5 for samples with ~15 nm nano-gaps. These high sensitivity, low cost nanostructures are now available on a commercial scale.

Contact Information

Moxtek, Inc.
452 W 1260 N
Orem, UT 84057, USA
www.moxtek.com

Matthew George
Applications Scientist
mgeorge@moxtek.com
+1, (801) 717-4187

References

[1] George, M.C., et al., "Wafer-scale Plasmonic and Photonic Crystal Sensors," Proc. SPIE 9547, Metallic Nanostructures and Their Optical Properties XIII, 95471F (2015). doi:10.1117/12.2188631

[2] Mashev, L., Popov, E., "Zero order anomaly of dielectric coated gratings," Opt. Commun. 55, 377-380 (1985).

[3] Cunningham, B.T., Li, P., Bo, L., Pepper, J., "Colorimetric Resonant Reflection as a Direct Biochemical Assay Technique," Sens. Actuator B 81, 316-328 (2002).

[4] Gallegos, D., et al., "Label-free biodetection using a smartphone," Lab Chip 13, 2124-2132 (2013).

[5] Cunningham, B.T., et al., "Label-Free Assays on the BIND System," Journal of Biomolecular Screening 9, 481-490 (2004)

[6] Block, I.D., et al., "A detection instrument for enhanced fluorescence and label-free imaging on photonic crystal surfaces," Optics Express 17, 13222-13235 (2009).

[7] Choi, C.J., et al., "Comparison of label-free biosensing in microplate, microfluidic, and spot-based affinity capture assays," Analytical Biochemistry 405, 1-10 (2010)

[8] Cunningham, B.T., "Photonic Crystal Surfaces as a General Purpose Platform for Label-Free and Fluorescent Assays," JALA 15, 120-135 (2010).

[9] Long, K.D., Yu, H., Cunningham, B.T., "Smartphone instrument for portable enzyme linked immunosorbent assays," Biomed. Opt. Express 5, 3792-3806 (2014).

[10] Mathias, P.C., Wu, H.-Y., Cunningham, B.T., "Employing two distinct photonic crystal resonances to improve fluorescence enhancement," APL 95, 021111 (2009).

[11] Wu, H.-Y., Cunningham, B.T., "Point-of-care detection and real-time monitoring of intravenously delivered drugs via tubing with an integrated SERS sensor," Nanoscale 6, 5162-5171 (2014).

[12] Wu, H.-Y., Choi, C.J., Cunningham, B.T., "Plasmonic Nanogap-Enhanced Raman Scattering Using a Resonant Nanodome Array," Small 8, 2878-2885 (2012).

[13] Choi, C.J., et al., "Biochemical sensor tubing for point-of-care monitoring of intravenous drugs and metabolites," Lab Chip 12, 574-581 (2012).

[14] Choi, C.J., et al., "Surface-enhanced Raman nanodomes," Nanotechnology 21, 415301 (2010).